

Array of Bose-Einstein condensates under time-periodic Feshbach-resonance management

F. Kh. Abdullaev^{a,b}, E. N. Tsoy^{a *}, B. A. Malomed^c, and R. A. Kraenkel^b

^a *Physical-Technical Institute of the Uzbek Academy of Sciences,*

2-B, Mavlyanov street, Tashkent, 700084, Uzbekistan

^b *Instituto de Fisica Teorica, UNESP, R. Pamplona 145,
01405-900 Sao Paulo, Brazil*

^c *Department of Interdisciplinary Studies, Faculty of
Engineering, Tel Aviv University, Tel-Aviv 69978, Israel*

(November 1, 2018)

The dynamics of a discrete soliton in an array of Bose-Einstein condensates under the action of a periodically time-modulated atomic scattering length (“Feshbach-resonance management, FRM”) is investigated. The cases of both slow and rapid modulation, in comparison with the tunneling frequency, are considered. We employ a discrete variational approach for the analysis of the system. The existence of nonlinear resonances and chaos is predicted at special values of the driving frequency. Soliton splitting is observed in numerical simulations. In the case of the rapid modulation, we derive an averaged equation, which is a generalized discrete nonlinear Schrödinger equation, including higher-order effective nonlinearities and intersite nonlinear interactions. Thus the predicted discrete FRM solitons are a direct matter-wave analog of recently investigated discrete diffraction-managed optical solitons.

03.75.Lm, 42.65.Wi, 05.45.-a

I. INTRODUCTION

Discrete solitons in nonlinear lattices with periodically varying parameters have recently attracted much attention. System belonging to this type include arrays of optical waveguides subject to periodic diffraction management^{1,2} and waveguide arrays with a periodic modulation of the tunnel-coupling constant³. The corresponding model is typically based on the discrete nonlinear Schrödinger (DNLS) equation, with the coefficient in front of the second-order finite-difference term varying along the propagation distance (formally, it looks like periodic time modulation of the coefficient). It was shown that, in the case of rapid and strong variations of the coupling constant, a stable breathing discrete soliton can exist² (the so-called diffraction-managed soliton). On the other hand, application of a relatively slow weak or moderate modulation at a resonant frequency results in a splitting of the discrete soliton³.

In periodically modulated DNLS systems of another type, the coefficient of the on-site cubic nonlinearity is subject to the modulation. In terms of nonlinear optics, these may be arrays of waveguides which have a layered structure, with the strength⁴, or even sign⁵, of the nonlinearity alternating between layers. An alternative, and actually more straightforward, physical realization of this type of the lattice is offered by an array of droplets of a Bose-Einstein condensate (BEC) trapped in a deep optical lattice^{6,7}, with the BEC scattering length oscillating in time. The latter type of the time-modulation may be provided by an ac magnetic field tuned to the Feshbach resonance, as it was predicted theoretically⁸ and demonstrated experimentally⁹. By analogy with the well-known techniques of the dispersion management¹⁰ and the above-mentioned diffraction management¹ in nonlinear optics, this time-modulation technique, applied to BEC, may be called Feshbach-resonance management (FRM). Very recently, it has been demonstrated that FRM provides for an effective mechanism of stabilization of two-dimensional BECs, even in the absence of the dc-magnetic-field trap¹¹. One-dimensional solitons subject to the action of FRM were also recently studied, which reveals stable breathers oscillating between the Gaussian and Thomas-Fermi shapes, and stable breathers of other types¹².

The aim of the present work is to consider the dynamics of solitons in the one-dimensional DNLS model with the nonlinearity subject to periodic modulation. We will treat the cases of both relatively slow and rapid modulations. In the former case, we will apply an analytical variational approximation (VA), which was developed for one-dimensional lattice models in Ref.¹³, and direct simulations, to study resonances and splitting in the discrete-soliton dynamics

*Corresponding author, e-mail: etsoy@physic.uzsci.net

(a recent review of the VA technique can be found in Ref.¹⁴). In the latter case, using the multiscale method¹⁵, we will derive an averaged equation, which has the form of a generalized DNLS equation with new nonlinear on-site and inter-site terms. Using this equation and VA, we will analyze the structure of average discrete-soliton solutions.

II. THE MODEL

We formulate the model in terms of a BEC trapped in a deep optical lattice, which is created by the interference of two counterpropagating optical beams. The dynamics of a BEC is governed by the Gross-Pitaevskii equation¹⁶:

$$i\hbar \frac{\partial \psi}{\partial t} = -\frac{\hbar^2}{2m} \Delta \psi + V(\mathbf{r})\psi + g(t)|\psi|^2\psi, \quad (1)$$

where $V(\mathbf{r}) = V_0(x, y) \sin^2(kz)$ is the optical potential, and $g(t) = 4\pi\hbar^2 a_s(t)/m$. Here a_s is the time-varying atomic scattering length, and m is the atomic mass. As it was mentioned above, the time dependence of a_s can be induced by ac magnetic field (or laser radiation with a time-modulated intensity) applied to the condensate. Due to the periodicity of $V(\mathbf{r})$, for a weakly coupled array of BECs, one can present a solution as

$$\psi = \sum_n u_n(t) \Phi(\mathbf{r} - \mathbf{r}_n), \quad (2)$$

where the function $\Phi(\mathbf{r} - \mathbf{r}_n)$ is assumed to be strongly localized around n -th site. Substituting Eq. (2) into Eq. (1), integrating over the transverse coordinates, and taking into account the exchange integrals only for neighboring sites, one arrives at a DNLS equation with a variable coefficient in front of the nonlinear term^{6,7}:

$$i\dot{u}_n + \frac{1}{2}(u_{n+1} + u_{n-1} - 2u_n) + a(t)|u_n|^2 u_n = 0. \quad (3)$$

Here the overdot stands for the time derivative, time is made dimensionless by means of the rescaling $t \rightarrow t\hbar/K$, where K is the tunnel-coupling parameter between adjacent wells in the optical lattice^{6,7}, and

$$a(t) = a_0 + a_1 \sin(\omega t) \quad (4)$$

is a coefficient proportional to minus the atomic scattering length in the BEC. Equation (3) describes the dynamics restricted within the lowest Bloch zone. Account of inter-zone transitions requires an extension of the DNLS model¹⁷.

Though the BEC system described above is the most relevant physical realization of Eq. (3), the same model also applies to an array of periodically modulated optical waveguides, with t being the propagation distance, rather than time. Without loss of generality, one can set $a_0 = 1$ and $a_0 = -1$ in Eq. (4) for the cases of the negative and positive scattering lengths (repulsion and attraction between atoms), respectively. The wave function $u_n(t)$ is normalized so that the dynamical invariant of Eq. (3),

$$W = \sum_{n=-\infty}^{\infty} |u_n|^2, \quad (5)$$

is the total number of particles. The characteristic length of the system $2\pi/k \sim 1 \mu\text{m}$, $V_0 \approx \hbar^2 k^2/m$, and the atomic population in each well is $\sim 10^3$ atoms. The characteristic frequency for the tunneling between wells is $\Omega_L = K/\hbar \sim 10$ Hz, and the separation between the energy levels in a single well is $\Omega \gtrsim 100$ Hz. Therefore, it makes sense to consider the variation of the driving frequency ω in the interval $\Omega_L < \omega K/\hbar < \Omega$.

First, we consider stationary pulse-shaped solutions of the unperturbed DNLS equation with $a_1 = 0$ in Eq. (4) in the form (see, e.g., Ref. ^{18,19})

$$u_n(t) = Q_n \exp(i\kappa n - i\chi t), \quad (6)$$

where κ is a wave number and χ is a frequency. As it follows from the dispersion relation for the linearized equation (3), a localized solution with the maximum of Q_n centered at some fixed point exists only for particular values of κ at which the group velocity vanishes, so we take $\kappa = 0$ for $a_0 = 1$, or, equivalently, $\kappa = \pi$ for $a_0 = -1$.

The fundamental soliton for $a_0 = 1$ was studied in detail as a numerical solution to the nonlinear eigenvalue problem with zero boundary conditions¹⁸⁻²⁰ (see also a review in Ref.²¹). In the case of $a_0 = -1$, solitons are *staggered*²⁰, with the π phase difference between adjacent sites; thus, on the contrary to the continuum nonlinear Schrödinger (NLS)

equation, the DNLS model supports stable bright solitons for either sign (repulsion or attraction) of the nonlinear interaction.

For convenience, here we briefly recapitulate basic properties of DNLS solitons. Parameters of the discrete soliton (6), found numerically from the nonlinear eigenvalue problem¹⁸, are shown by points in Fig. 1. The left axis in Fig. 1(a) pertains to the inverse width α , which was found by matching the soliton's tail to the asymptotic expression $|u_n| = A \exp(-\alpha|n|)$, where A is the soliton's amplitude [cf. Eq. (9) below]. The right axis in Fig. 1(b) corresponds to the pulse's area, which we define as $S = \sum_n |u_n|$. The dependencies for $a_0 = -1$ have the same form, with the only difference that χ is shifted so that $\chi \rightarrow 2 - \chi$. Since W , χ and α are monotonic functions of A , the stationary solution (6) is defined by fixing of any one of these parameters.

Similarly to the case of the continuum NLS equation, the addition of chirp to the soliton (6) (*chirp imprinting*) splits it into two separating soliton-like pulses, if the chirp b exceeds a critical (threshold) value b_{th} (detailed consideration of a similar problem in the continuum NLS equation was given in Ref.²²). We introduce the chirp by taking an initial condition as

$$u_n(0) = Q_n \exp(ib|n|) \quad (7)$$

(the value of b is restricted to the interval $[-\pi, \pi]$). The dependence of b_{th} on the amplitude A of the unperturbed DNLS soliton is presented in Fig. 2.

In fact, the curves shown in Fig. 2 diverge at sufficiently large A . The meaning of this is that, if the soliton's amplitude A exceeds the value 1.66, the initial pulse with any amount of chirp gives rise to a soliton centered at $n = 0$, while other parts of the initial pulse split off from it and move in opposite directions.

It is possible to understand the chirp-induced splitting of the pulse into two in the following way. The original chirped pulse (7) may be regarded as a superposition of two pulses which carry the phase gradient of opposite signs (cf. a similar model developed in the framework of the continuum NLS equation in Ref.²²). As is known, the velocity of an isolated soliton is generated by its phase gradient. Since the two constituents of the overall chirped pulse are originally close to each other, the attraction between them is strong enough to keep them together. However, the increase of b leads to increase of the opposite phase-gradient thrusts applied to the constituents, and finally to splitting between them.

III. THE VARIATIONAL APPROXIMATION AND DIRECT SIMULATIONS IN THE CASE OF SLOW MODULATIONS

A. The general formalism of the variational approximation

The DNLS equation (3) is derived from the Lagrangian,

$$L = \sum_{n=-\infty}^{\infty} \frac{i}{2} (u_n^* \dot{u}_n - u_n \dot{u}_n^*) - \frac{1}{2} |u_{n+1} - u_n|^2 + \frac{1}{2} a(t) |u_n|^4. \quad (8)$$

Following Ref.¹³, we base the variational approximation (VA) for the soliton governed by Eq. (3) on the following *ansatz*:

$$u_n(t) = A \exp(i\phi + ib|n| - \alpha|n|), \quad (9)$$

where A , ϕ , b , and α are real functions of time. Substituting the ansatz (9) into Eq. (8), one can easily calculate the corresponding *effective Lagrangian* in a form

$$\frac{L}{W} = -\frac{1}{\sinh(2\alpha)} \frac{db}{dt} + \frac{\cos b}{\cosh \alpha} + \frac{1}{4} W a(t) \frac{\sinh \alpha}{\cosh^3 \alpha} \cosh(2\alpha), \quad (10)$$

where

$$W = A^2 \coth \alpha, \quad (11)$$

is a dynamical invariant, which coincides with the total number of particles, obtained by substitution of the ansatz (9) into Eq. (5). We mention that a term in the full Lagrangian from which it follows that $dW/dt = 0$ contains the

phase derivative $\dot{\phi}$ [which gives the frequency $-\chi$ in the stationary state, see Eq. (6)]. That term was dropped in the expression (10), as it does not contribute to other variational equations. Finally, the variational equations for the soliton's chirp and inverse width are

$$\frac{db}{dt} = 2(\cos b) \frac{\sinh^3 \alpha}{\cosh(2\alpha)} - \frac{1}{2} W a(t) (\tanh^2 \alpha) \frac{2 \cosh(2\alpha) - 1}{\cosh(2\alpha)}, \quad (12)$$

$$\frac{d\alpha}{dt} = -(\sin b) (\sinh \alpha) \tanh(2\alpha). \quad (13)$$

B. Revisiting the stationary model

First, we dwell on the unperturbed case, with $a(t) = \text{const} \equiv a_0$ [cf. Eq. (4)]. In the case, all the points with $\alpha = 0$ and $b = \text{const}$ are stationary solutions, i.e., fixed points (FPs). However, they do not correspond to localized waves, therefore they are formal solutions. Further, it is easy to see that Eqs. (12) and (13) give rise to nontrivial FPs with $b_{\text{FP}} = 0$ for $a_0 = 1$, and $b_{\text{FP}} = \pi$ for $a_0 = -1$, the corresponding value α_{FP} being defined by the equation¹³

$$\sinh \alpha_{\text{FP}} = \frac{1}{4} W (1 + 3 \tanh^2 \alpha_{\text{FP}}). \quad (14)$$

The parameters of the FP, which corresponds to stationary discrete soliton (6), are shown by solid lines in Fig. 1. As is seen, the results of the VA are in good agreement with the exact numerical solution of Eq. (3). Deviation in S (area of the pulse) indicates that the VA is not applicable in the limit of small A . This is clear because this limit corresponds to the continuum system, whose stationary soliton solution differs from the ansatz (9).

Linearization of Eqs. (12) and (13) around the FP yields a squared frequency of small oscillations,

$$\begin{aligned} \omega_0^2 = & \frac{\sinh^3(\alpha_{\text{FP}}) \cosh^2(\alpha_{\text{FP}})}{\cosh^3(2\alpha_{\text{FP}})} \\ & \times \{ 4 \sinh(\alpha_{\text{FP}}) [\cosh(2\alpha_{\text{FP}}) + 2] \\ & - \frac{W}{\cosh^4(\alpha_{\text{FP}})} [5 \cosh^2(2\alpha_{\text{FP}}) - 2 \cosh(2\alpha_{\text{FP}}) - 1] \}. \end{aligned} \quad (15)$$

Using Eq. (14), one can show that ω_0^2 given by Eq. (15) is always positive, i.e., VA does not predict any (artificial) instability. The dependence of ω_0 on A , obtained from Eq. (15), is shown by a solid line in Fig. 3. In the same figure, crosses show resonant values of the frequency found from numerical simulations of Eq. (3) with a small coefficient a_1 in front of the variable part of the nonlinearity coefficient, see Eq. (4). In the simulations, the forcing frequency ω was varied at the fixed small a_1 , with the purpose to identify a value that generated strongest resonant response. The relative difference between the thus found resonance frequency and the value predicted by Eq. (15) is about 0.1, and the overall behavior of the curves is identical. It is worthy to note that ω_0 almost coincides with the soliton's frequency $|\chi|$. Thus, the results presented in Figs. 1 and 3 justify the validity of the VA based on the ansatz (9).

The phase plane of Eqs. (12) and (13) for $a_0 = 1$ and $a_1 = 0$ is shown in Fig. 4(a), where arrows point out a direction of motion along a trajectory. The phase plane for the case of $a_0 = -1$ is obtained by the shift $b \rightarrow \pi - b$, while that for the case $a_0 = 0$ is obtained by setting $\alpha_{\text{FP}} \rightarrow 0$. As it follows from here, the stable FP, which corresponds to the discrete soliton, exists for *either* sign of a_0 , and vanishes if $a_0 = 0$. As it also follows from Fig. 4(a), the evolution initiated by the initial condition with $\alpha(0) = \alpha_{\text{FP}}$ and small $b(0)$ corresponds to oscillations near the FP. However, for large values of $|b(0)|$, the asymptotic value of $\alpha(t)$ at $t \rightarrow \infty$ tends to zero. This fact is in qualitative agreement with the above-mentioned result that the addition of a chirp may destroy the soliton.

C. The variational approximation for the nonstationary model

We now proceed to the case of the ac-driven system, with $a_1 \neq 0$. If a_1 is small, strong response of the system to the time-periodic modulation is expected when the modulation frequency ω is close to the eigenfrequency ω_0 of the internal oscillations of the soliton in the unperturbed system, which is given by Eq. (15); in fact, the resonant response was already taken into regard when collecting the data shown by crosses in Fig. 3. Moreover, the dynamics is expected to become chaotic, via the resonance-overlapping mechanism, if the modulation amplitude a_1 exceeds some threshold value.

The Poincaré map illustrating a typical example of the chaotic behavior, as found from the numerical solution of Eqs. (12) and (13), is presented in Fig. 4(b). Shown are the discrete trajectories initiated by sets of the initial conditions, namely, the one with $(b_1, \alpha_1) = (0, 0.789)$, that corresponds to the stationary discrete soliton with $A = 1$ in the unperturbed system ($a_1 = 0$), and $(b_2, \alpha_2) = (0.13, 0.74)$. The modulation frequency ω is close to the eigenfrequency of small oscillations ω_0 . For the former initial condition, the point in the space (b, α) is chaotically moving away from the unperturbed FP. However, the chaotic evolution is a transient feature, as the point eventually moves so that $\alpha(t)$ asymptotically tends to zero, implying infinite broadening of the soliton.

As for the second set of initial conditions, a new FP is found in a vicinity of the unperturbed one. This new FP predicts the existence of quasi-stationary discrete FRM solitons in the case of the slow modulation. Similar behavior near the corresponding stationary point is observed for the case $a_0 = -1$.

D. Direct simulations

We have performed systematic comparison of the predictions produced by the VA against direct simulations of the full DNLS equation (3). The simulations show that, generally speaking, VA correctly predicts only an initial stage of the dynamics. The radiation of linear waves by a soliton, which is ignored by the VA, gives rise to an effective dissipation, that makes the resonance frequency different from ω_0 . Furthermore, since ω_0 depends on W , and the radiation loss results in gradual decrease of W , the soliton decouples from the resonance. In principle, VA might be made more accurate by adding a radiation mode (“tail”) to the ansatz, cf. the analysis developed in Ref.²³ for the soliton in the continuum NLS equation (see also the review¹⁴), but we do not aim to develop such an involved generalization of the VA in the present work. In any case, a conclusion is that the dynamics of the discrete soliton, as found from direct numerical simulation of Eq. (3) for $a_1 \lesssim 0.05$, is close to that predicted by the variational equations (12) and (13). Namely, oscillations of the soliton’s parameters are regular for very small modulations, and become chaotic when a_1 exceed a threshold, see below.

Typical examples of the soliton dynamics with $\omega = 0.5$ and different values of the modulation amplitude a_1 are displayed in Fig. 5. An important observation, which is not predicted at all by the single-soliton ansatz, is *splitting* of the pulse, which is observed in Fig. 5(b). Note that for other values of a_1 , in Figs. 5(a) and 5(c), a stable soliton is observed, centered at $n = 0$, whose parameters oscillate because of the modulation. Therefore, the splitting which occurs at $a_1 \gtrsim 0.1$ is due to an interplay between the soliton itself, its intrinsic eigenmodes, and the energy exchange with radiation modes (continuous spectrum). It is noteworthy that the splitting is qualitatively similar to that revealed by direct simulations of the continuum NLS equation with a term accounting for periodic modulation of the linear dispersion term [whose discrete counterpart is the finite-difference combination in Eq. (3)], which was reported in Ref.²⁴. A similar phenomenon was also observed in the discrete model with the finite-difference term subject to periodic modulation³.

Results of the systematic numerical study of the splitting of the pulse with the initial amplitude $A = 1$ are summarized in Fig. 6. In the simulations, absorbing boundary conditions, were used, the total number of particles was $N \geq 200$, and the dimensionless simulation time was, at least, $60\pi/\omega$. We classify as splitting cases when at least two pulses emerge, moving in opposite directions, and no pulse with an appreciable amplitude stays around $n = 0$. For $a_1 \gtrsim 0.2$, the modulation results in generation of several moving pulses. However, if a soliton with conspicuous amplitude is eventually found around $n = 0$, this case was classified as a “stable soliton”.

Figure 6 also displays the dependence of a threshold amplitude a_1 , past which the initial state chaotically drifts to $\alpha = 0$, versus ω is also presented, as found from simulations of Eqs. (12) and (13). As is seen, the splitting actually occurs far above the threshold in a region of the developed dynamical chaos. The diagram for the case $a_0 = -1$ looks similar, but not exactly the same.

IV. THE AVERAGED EQUATION FOR THE CASE OF RAPID MODULATIONS

In this section we consider the case of high-frequency modulations, with $\epsilon \equiv 1/\omega \ll 1$. Note that we do not require a_1 to be small. In this case, it is natural to use the multiscale method^{15,11}. To this end, we introduce a set of time scales $\tau = t/\epsilon$, $t_k = \epsilon^k t$, where $k = 0, 1, 2, \dots$, and look for a solution in the form

$$u_n = U_n + \epsilon u_n^{(1)} + \epsilon^2 u_n^{(2)} + \dots \quad (16)$$

We substitute Eq. (16) into Eq. (3) and collect terms at the same order in ϵ . Then, at order ϵ^0 we obtain

$$i\frac{\partial U_n}{\partial t_0} + i\frac{\partial u_n^{(1)}}{\partial \tau} + \frac{1}{2}(U_{n+1} + U_{n-1} - 2U_n) + a(\tau)|U_n|^2U_n = 0, \quad (17)$$

where $a(\tau) \equiv a(t/\epsilon)$, and U_n is a function of the slow variables t_k . After averaging in the fast variable τ , one has

$$i\frac{\partial U_n}{\partial t_0} + \frac{1}{2}(U_{n+1} + U_{n-1} - 2U_n) + a_0|U_n|^2U_n = 0, \quad (18)$$

where $a_0 \equiv \langle a(\tau) \rangle$ standing for the average value of the variable coefficient $a(\tau)$. Then the equation for first correction $u_n^{(1)}$ takes the form

$$i\frac{\partial u_n^{(1)}}{\partial \tau} = -[a(t) - a_0] |U_n|^2U_n,$$

a solution to which is

$$u_n^{(1)} = i(\mu_1 - \langle \mu_1 \rangle) |U_n|^2U_n,$$

where $\mu_1 \equiv \int_0^\tau [a(x) - a_0]dx$, and $\langle \dots \rangle$ again stands for the average value.

At order ϵ^1 , we obtain $\partial U_n / \partial t_1 = 0$, and

$$\begin{aligned} u_n^{(2)} &= (\mu_2 - \langle \mu_2 \rangle) [|U_n|^2(U_{n+1} + U_{n-1}) - \\ &\frac{1}{2}U_n^2(U_{n+1}^* + U_{n-1}^*) - \frac{1}{2}|U_{n+1}|^2U_{n+1} - \frac{1}{2}|U_{n-1}|^2U_{n-1}] \\ &- \frac{1}{2}[(\mu_1 - \langle \mu_1 \rangle)^2 - 2M]|U_n|^4U_n, \end{aligned}$$

where $\mu_2 \equiv \int_0^\tau [\mu_1(x) - \langle \mu_1 \rangle]dx$, and $M = (\langle \mu_1^2 \rangle - \langle \mu_1 \rangle^2)/2$. Finally, at order ϵ^2 we find

$$\begin{aligned} \frac{\partial U_n}{\partial t_2} &= iM[|U_{n+1}|^2(2|U_n|^2U_{n+1} + U_n^2U_{n+1}^*) + \\ &|U_{n-1}|^2(2|U_n|^2U_{n-1} + U_n^2U_{n-1}^*) - \\ &3|U_n|^4(U_{n+1} + U_{n-1})] + 2iMa_0|U_n|^6U_n \end{aligned} \quad (19)$$

Substituting Eqs. (18) and (19) into the relation

$$\frac{\partial U_n}{\partial t} = \frac{\partial U_n}{\partial t_0} + \epsilon \frac{\partial U_n}{\partial t_1} + \epsilon^2 \frac{\partial U_n}{\partial t_2} + \dots,$$

one can derive the averaged equation,

$$\begin{aligned} i\dot{U}_n + \frac{1}{2}(U_{n+1} + U_{n-1} - 2U_n) + a_0|U_n|^2U_n &= \\ -2Ma_0\epsilon^2|U_n|^6U_n - M\epsilon^2 & \\ \times [|U_{n+1}|^2(2|U_n|^2U_{n+1} + U_n^2U_{n+1}^*) + & \\ |U_{n-1}|^2(2|U_n|^2U_{n-1} + U_n^2U_{n-1}^*) - & \\ 3|U_n|^4U_{n+1} - 3|U_n|^4U_{n-1}] , & \end{aligned} \quad (20)$$

where $M \equiv a_1^2/4$ for the case of the periodic modulation in Eq. (4).

Equation (20) is the higher-order DNLS equation produced by the averaging procedure, which contains extra on-site and intersite (nonlocal) nonlinearities. A change of variables $q_n \equiv U_n + \epsilon^2 M |U_n|^4 U_n$ allows to rewrite Eq. (20), retaining only terms up to $O(\epsilon^2)$, in the following form

$$\begin{aligned} i\dot{q}_n + \frac{1}{2}(q_{n+1} + q_{n-1} - 2q_n) + a_0|q_n|^2q_n &= \\ \frac{1}{2}\epsilon^2 M [3|q_n|^4(q_{n+1} + q_{n-1}) + 2|q_n|^2q_n^2(q_{n+1}^* + q_{n-1}^*) + & \\ |q_{n+1}|^4q_{n+1} + |q_{n-1}|^4q_{n-1}] - & \\ \epsilon^2 M [|q_{n+1}|^2(2|q_n|^2q_{n+1} + q_n^2q_{n+1}^*) + & \\ |q_{n-1}|^2(2|q_n|^2q_{n-1} + q_n^2q_{n-1}^*)] . & \end{aligned} \quad (21)$$

An advantage of the equation in the form (21) is that it can be derived from a Lagrangian,

$$L_q = L_0 - \frac{1}{2}\epsilon^2 M \sum_{n=-\infty}^{\infty} (|q_{n+1}|^2 - |q_n|^2)^2 \times (q_n^* q_{n+1} + q_n q_{n+1}^*), \quad (22)$$

where L_0 is obtained from the underlying Lagrangian (8) by the substitution $u_n \rightarrow q_n$ and $a(t) \rightarrow a_0$. The existence of the Lagrangian L_q allows one to apply the variational approximation (VA) like in Section III.

For the application of VA, we take the ansatz for q_n in the form

$$q_n = B \exp(i\psi + ic|n| - \beta|n|), \quad (23)$$

cf. Eq. (9). Substituting Eq. (23) into Eq. (22), we calculate the effective Lagrangian,

$$L_q = L_0 - 4\epsilon^2 MW_q^3 \cos(c) \frac{\sinh^2(\beta) \tanh^3(\beta)}{\sinh(3\beta)}.$$

Here L_0 is the same expression as in Eq. (10), with a change $b \rightarrow c$, $\alpha \rightarrow \beta$, $W \rightarrow W_q = B^2 \coth(\beta)$, and $a(t) \rightarrow a_0$. Now one can deduce a dynamical system for the variable c and β similar to Eqs. (12) and (13). The fixed point $(\beta_{\text{FP}}, 0)$ for $a_0 = 1$, or (β_{FP}, π) for $a_0 = -1$, of this system represents a FRM soliton in the case of rapid modulations, where β_{FP} is to be found from the equation

$$\begin{aligned} & \sinh(\beta_{\text{FP}}) - \frac{W_q}{4} [1 + 3 \tanh^2(\beta_{\text{FP}})] + \\ & 4 \text{sign}(a_0) \epsilon^2 MW_q^2 \sinh(\beta_{\text{FP}}) \tanh^2(\beta_{\text{FP}}) \\ & \times \frac{[10 + 15 \cosh(2\beta_{\text{FP}}) - \cosh(4\beta_{\text{FP}})]}{[1 + 2 \cosh(2\beta_{\text{FP}})]^2} = 0. \end{aligned} \quad (24)$$

The norm \bar{W} and amplitude \bar{A} of the field U_n in the averaged soliton are related to those of the field q_n as

$$\begin{aligned} \bar{W} & \approx W_q [1 - 2\epsilon^2 MW_q^2 (\tanh^3 \beta) \coth(3\beta)], \\ \bar{A} & \approx A_q (1 - \epsilon^2 MA_q^4). \end{aligned} \quad (25)$$

The dependence $\bar{W}(\bar{A})$ found from Eqs. (24) and (25) at different values of $\delta \equiv a_1^2/(4\omega^2)$ is displayed in Fig. 7. Different curves in the figure terminate at finite values of \bar{A} because the relation (25), as well as the change of variables $U_n \rightarrow q_n$, are not valid outside the corresponding intervals. As it is suggested by Fig. 7, one can effectively control the soliton by an appropriate choice of the modulation parameters. Increase of the total number of particles in the averaged soliton, as compared to that in the unperturbed soliton with the same amplitude, is clearly seen in Fig. 7.

V. CONCLUSIONS

We have studied the dynamics of an array of Bose-Einstein condensates with the time-dependent scattering length. Applying the variational approximation, the frequency ω_0 of small intrinsic oscillations of the soliton was predicted. The possibility of chaotic dynamics in the near-resonance case, when the driving frequency ω is close to ω_0 , was shown. Direct simulations have demonstrated that the modulations of sufficient strength may result in splitting of the soliton. Results of the simulations were summarized in the form of the diagram which shows the splitting regions in the (ω, a_1) plane. The existence of stable Feshbach-resonance-managed discrete matter-wave solitons was demonstrated in the cases of both slow and rapid modulation of the nonlinearity coefficient. In the latter case, the soliton dynamics reduces to the generalized DNLS equation, which involves additional on-site and inter-site nonlinearities. By making use of this equation, properties of the averaged soliton were predicted. In particular, increase of the total number of atoms in this soliton in comparison with the ordinary discrete soliton of the same amplitude was shown.

The *chirp imprinting* discussed in Sect. II can be an effective tool, similar to the phase-engineering method²⁵, for manipulating the condensate's wave function. Pulse splitting induced by the chirp imprinting, or otherwise by the application of Feshbach-resonance modulation, can be used as a source of coherent pulse pairs in an atomic Mach-Zehnder interferometer²⁶.

ACKNOWLEDGEMENT

B. A. M. appreciates hospitality of Instituto de Fisica Teorica at UNESP (Sao Paulo, Brazil). F. Kh. A. is grateful to FAPESP for the partial support of this work.

- ¹ H. S. Eisenberg, Y. Silberberg, R. Morandotti, and J. S. Aitchison, *Phys. Rev. Lett.* **85**, 1863 (2000).
- ² M. J. Ablowitz and Z. H. Musslimani, *Phys. Rev. Lett.* **87**, 254102 (2002).
- ³ U. Peschel and F. Lederer, *J. Opt. Soc. Am. B* **19**, 544 (2002).
- ⁴ L. Berge, V. K. Mezentsev, J. J. Rasmussen, P. L. Christiansen, and Yu. B. Gaididei, *Opt. Lett.* **25**, 1037 (2000).
- ⁵ I. Towers and B. A. Malomed, *J. Opt. Soc. Am. B* **19**, 537 (2002).
- ⁶ F. Kh. Abdullaev, B. B. Baizakov, S. A. Darmanyan, V. V. Konotop, and M. Salerno, *Phys. Rev. A* **64**, 043606 (2001).
- ⁷ A. Trombettoni and A. Smerzi, *Phys. Rev. Lett.* **86**, 2353 (2001).
- ⁸ Y. Kagan, E. L. Surkov, and G. V. Shlyapnikov, *Phys. Rev. Lett.* **79**, 2604 (1997).
- ⁹ S. L. Cornish, N. R. Claussen, J. L. Roberts, E. A. Cornell, and C. E. Wieman, *Phys. Rev. Lett.* **85**, 1795 (2000).
- ¹⁰ M. Suzuki et al., *Electron. Lett.* **31**, 2027 (1995); N. J. Smith et al., *Electron. Lett.* **32**, 54 (1996).
- ¹¹ F. Kh. Abdullaev, J. G. Caputo, R. A. Kraenkel, and B. A. Malomed, *Phys. Rev. A* **67**, 013605 (2003); H. Saito and M. Ueda, *Phys. Rev. Lett.* **90**, 040403 (2003).
- ¹² P. G. Kevrekidis, G. Theocharis, D. J. Frantzeskakis, and B. A. Malomed, “Feshbach-resonance management for Bose-Einstein condensates”, *Phys. Rev. Lett.* (2003), in press.
- ¹³ B. A. Malomed and M. I. Weinstein, *Phys. Lett. A* **220**, 91 (1996).
- ¹⁴ B. A. Malomed, *Progr. Opt.* **43**, 71 (2002).
- ¹⁵ T. S. Yang and W. L. Kath, *Opt. Lett.* **22**, 985 (1997).
- ¹⁶ See e.g. F. Dalfovo, S. Giorgini, L. P. Pitaevskii, and S. Stringari, *Rev. Mod. Phys.* **71**, 463 (1999).
- ¹⁷ G. L. Alfimov, P.G. Kevrekidis, V. V. Konotop, and M. Salerno, *Phys. Rev. E* **66**, 046608 (2002).
- ¹⁸ A. C. Scott, *Phys. Lett. A* **119** (1986).
- ¹⁹ A. B. Aceves, C. De Angelis, T. Peschel, R. Muschall, F. Lederer, S. Trillo, and S. Wabnitz, *Phys. Rev. E*, **53**, 1172 (1996).
- ²⁰ D. Cai, A. R. Bishop, and N. Grønbech-Jensen, *Phys. Rev. Lett.* **72**, 591 (1994).
- ²¹ P.G. Kevrekidis, K.Ø. Rasmussen, and A.R. Bishop, *Int. J. Mod. Phys. B* **15**, 2833 (2001).
- ²² D. J. Kaup, J. El-Reedy, and B. A. Malomed, *Phys. Rev. E* **50**, 1635 (1994).
- ²³ W. L. Kath and N. F. Smyth, *Phys. Rev. E* **51**, 1484 (1995).
- ²⁴ R. Grimshaw, J. He, and B. A. Malomed, *Phys. Scripta* **53**, 385 (1996).
- ²⁵ L. Dobrek, M. Gajda, M. Lewenstein, K. Sengstock, G. Birkl, and W. Ertmer, *Phys. Rev. A* **60**, R3381 (1999); B. P. Anderson, P. C. Haljan, C. A. Regal, D. L. Feder, L. A. Collins, C. W. Clark, and E. A. Cornell, *Phys. Rev. Lett.* **86**, 2926 (2001).
- ²⁶ S. Poetting, P. Meystre, and E. M. Wright, In “Nonlinear Photonic Crystals”, Eds. R.E. Slusher and B.J. Eggleton, (Springer Verlag, Berlin, 2003); see also arXiv: cond-mat/ 0009289 (2000).

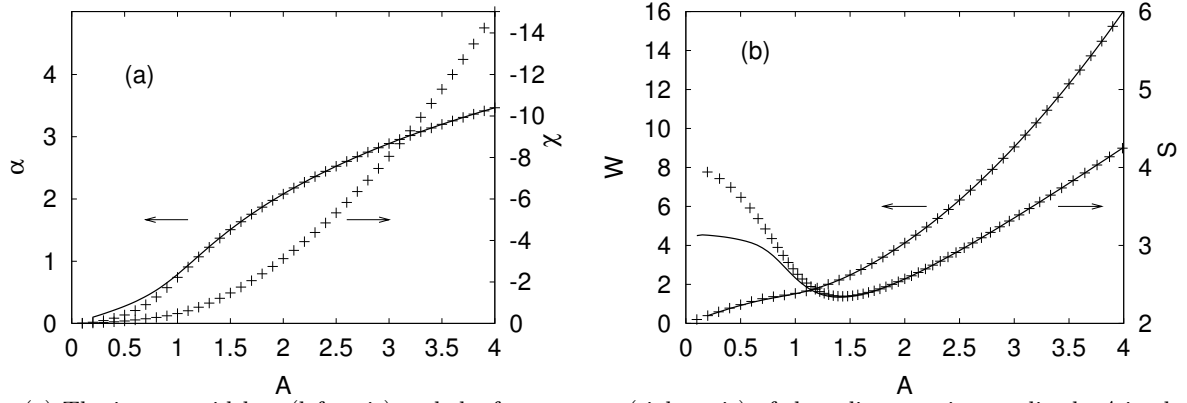


FIG. 1. (a) The inverse width α (left axis) and the frequency χ (right axis) of the soliton vs. its amplitude A in the DNLS model without the time-modulation, $a_0 = 1$. (b) The norm W (left axis) and the soliton's area S (right axis) vs. A . Point symbols represent data found from the numerical solution of the nonlinear eigenvalue problem; the solid lines are the prediction of the analytical variational approximation [see Eqs.(11) and (14)].

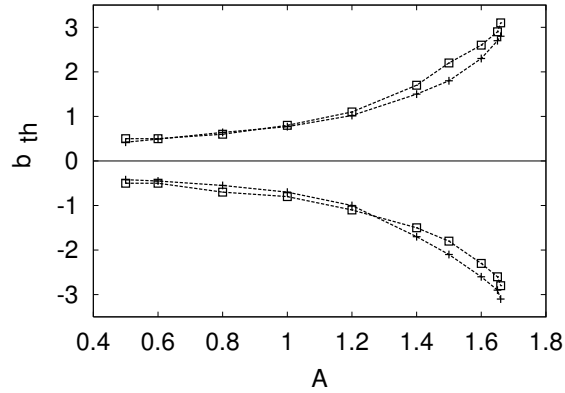


FIG. 2. The critical value of the chirp added to the fundamental discrete soliton, see Eq. (7), which splits the soliton into two separating pulses, vs. the amplitude of the unperturbed fundamental soliton. Squares (pluses) corresponds to $a_0 = 1$ ($a_0 = -1$).

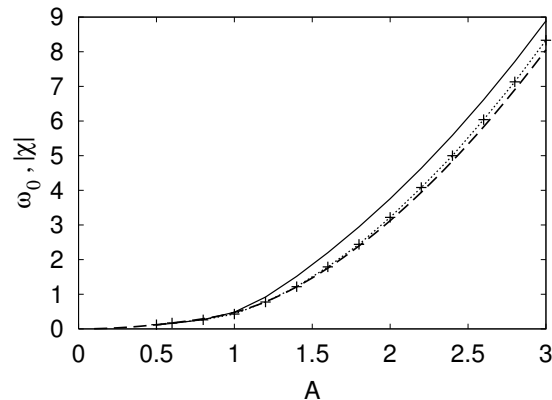


FIG. 3. The frequency of small intrinsic oscillations of the discrete solitons around the stationary configurations, in the case $a_0 = 1$, vs. the soliton's amplitude A . The solid line shows the frequency ω_0 as predicted, in the framework of the variational approximation, by Eq. (15). Points connected by the dotted line are values of the forcing frequency which produce a resonant response in numerical simulations of Eq. (3) with a small time-periodic forcing term added to it. For comparison, the dashed line shows the soliton's internal frequency $|\chi|$.

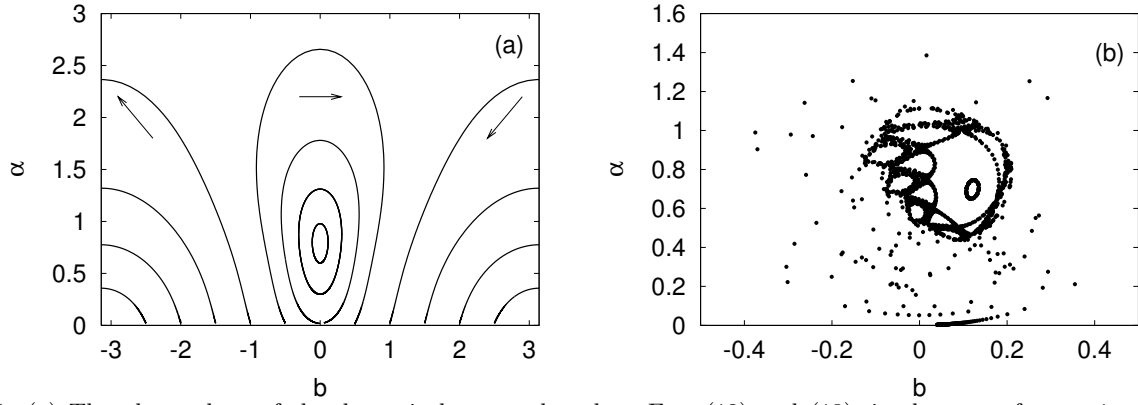


FIG. 4. (a) The phase plane of the dynamical system based on Eqs. (12) and (13), in the case of $a_0 = 1$, $a_1 = 0$, and $W = 1.5202$. Such a value of W corresponds to a soliton with $A = 1$. (b) An example of chaotic dynamics for the periodically-modulated system at $W = 1.5202$, $a_0 = 1$, $a_1 = 0.02766$ and $\omega = 0.481$.

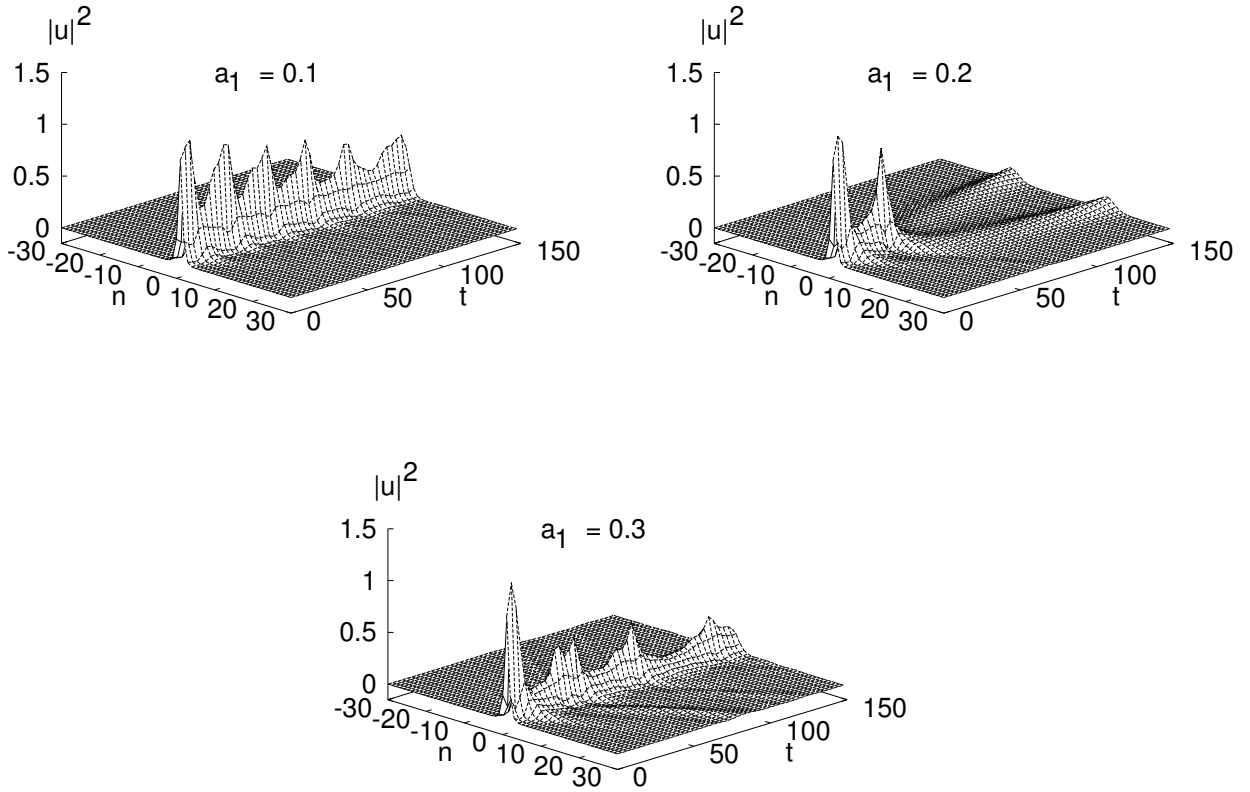


FIG. 5. Evolution of a discrete soliton with the initial amplitude $A = 1$ in the periodically modulated system with $a_0 = 1$, $\omega = 0.5$, and different values of a_1 .

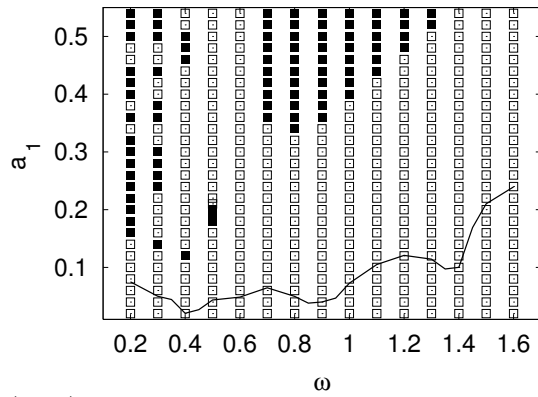


FIG. 6. The diagram in the plane (ω, a_1) , for the case $a_0 = 1$. Open and solid rectangles correspond to stable and splitting solitons, respectively. The initial soliton's amplitude is $A = 1$. The solid line is the chaos-onset threshold as predicted by the variational equations.

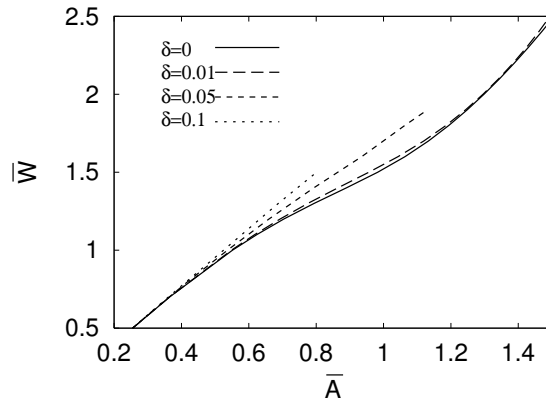


FIG. 7. The dependence of \bar{W} vs. \bar{A} of an average soliton (dashed lines) is compared with that of the unperturbed DNLS equation (solid line), $a_0 = 1$.